Communication Skills 2

Assigment 2: Writing

Numerical simulation of wound healing processes (Part I)

Lisandro Roldan, Pablo Sáez

Laboratori de Calcul Numeric (LaCaN), Universitat Politecnica de Catalunya, Barcelona, Spain.

January 9, 2017

Abstract

Gap closure of wounds in tissues is critical for the development of living organisms. It is achieved by a coordinated response of various mechanisms: once the gap is produced signals travel through the cells and the tissue respond mechanically to it in a non-linear way to close reduce the hole. In this paper we present a numerical approach to simulate the mechanical response of the tissue during the first stages of the wound healing process using a Neo-Hookean model with growth driven either by volume or density change.

Index terms— Biomechanics, Multiphysics, Electro-Mechanical Coupling

1 Introduction

Gaps in multicellular tissue naturally occur during the lifetime of an organism, from developmental stages to adult life. Holes within tissues may be natural consequences of physiological processes or an outcome of pathological or injurious events and result in ulcers and wounds. [4, 16, 17, 19, 27, 29, 30]

Closure of wounds and gaps in tissues is fundamental for the correct development and physiology of multicellular organisms and, when misregulated, may lead to inflammation and tumorigenesis [25]. That is why a clear understanding of this phenomena and the mechanisms involved is so important.

Properties like the ability to sense tension changes within the tissue, repair its defects, and elicit effective immune responses are coordinated and regulated in very robust ways from a very early point after injury and, most importantly, are highly conserved among different types of tissues. Therefore, studying wound healing in simple model systems can shed light on fundamental processes that ultimately might prove essential to our understanding of the more complex wound healing response observed in human tissues. [3]

A crucial step of the wound healing response is the restoration of a continuous epithelial layer to recover tissue homeostasis, regain barrier integrity, and protect organisms from infection [7]. Epithelial repair is achieved through the collective movement of wound-bordering cells into the wound bed. To account for this collective movement, two main mechanisms are commonly invoked [2, 15, 30]. The first one is the assembly of a supracellular actomyosin ring at the wound margin, whose contraction drives the wound edges together like a purse-string [6, 14, 20, 31] . The second mechanism is collective migration of marginal and submarginal cells led by lamellipodial and filopodial protrusions [8,9,22,23,32].

Before the wound shows any significant reduction of its area [3], a series of processes occur culminating in the formation of the actomyosin ring (see Figure 1)

Firstly, after wound induction is the displacement of tissue that surrounds the wound, causing a significant deformation of the cells and their contents. The cytoskeleton networks are stretched in the axis parallel to the wound margin and compressed in the perpendicular axis. Consequence of the mechanical stress that cells suffer is a dramatic increase in intracellular calcium. [3]

High levels of intracellular calcium affect many signaling pathways, but one of the proteins that it regulates, Gelsolin , seems to have an important role in the generation of new actin filaments. Gelsolin has actin filament - severing activity and its downregulation impairs the actin flow. Cytoskeleton deformation

together with the Gelsolin-severing activity create the appropriate combination of exposed barbed ends and released actin monomers that can trigger a rapid burst of forming dependent elongation of actin filaments that kicks off the actin flow. The distance from the wound margin at which this phenomenon occurs depends on the extent of tissue displacement. [3]

The step that follows the initial burst of actin filaments seems to be the recruitment of myosin motors that act on the filaments to initiate a flow of actomyosin and apical cell constriction that propagates toward the wound edge. The actomyosin flow is likely the result of local cycles of actomyosin assembly and contraction followed by disassembly and restoration of homeostatic levels. [3]

The goal of this work is to perform a numerical simulation of this early stage of the wound closure. It is important to note that the the formation of the actomyosin ring occur before any considerable closure of the wound occurs, and therefore in this stage the phenomena is considered coupled only in one direction for the simplicity of the model and in the late stages of the simulation they will be fully coupled.

2 Governing Equations

2.1 Kinematic equations

First, we reiterate the basic equations of the kinematically non-linear behavior. Our most important kinematic quantity is the deformation gradient $\mathbf{F}$, the tangent of the nonlinear deformation map φ, [24]

$$\mathbf{F} = \nabla_X \varphi. \tag{1}$$

Where the symbol ∇_X denotes the spatial gradient with respect to the referential coordinates $\mathbf{X}$. We can then introduce the Jacobian $J = det(\mathbf{F})$ and the right Cauchy Green deformation tensor, [24]

$$\mathbf{C} = \mathbf{F}^t \cdot \mathbf{F}. \tag{2}$$

To account for the characteristic quasi-incompressible behaviour of soft biological tissues, we adopt a volumetric-isochoric decomposition of the deformation gradient, [10, 11]

$$\mathbf{F} = \mathbf{J}^{1/3}\bar{\mathbf{F}} \tag{3}$$

The over-bar is associated with the prefix isochoric and denotes the volume-preserving part. Accordingly, $\bar{\mathbf{F}}$ denotes the isochoric deformation gradient with $det(\bar{\mathbf{F}}) = 1$, and [24]

$$\bar{\mathbf{C}} = \bar{\mathbf{F}}^t \cdot \bar{\mathbf{F}}. \tag{4}$$

denotes the associated isochoric right Cauchy Green deformation tensor. It is convenient to introduce the first and fourth invariants, [24]

$$\bar{I}_1 = \bar{\mathbf{C}} : \mathbf{I} \quad and \quad \bar{I}_4 = \bar{\mathbf{C}} : \mathbf{N} \tag{5}$$

where $\mathbf{N} = \mathbf{n} \otimes \mathbf{n}$ denotes the structural tensor defined in terms of the characteristic microstructural direction $\mathbf{n}$. [24]

2.2 Quasi-incompressibility Mechanics

Second, we summarize the basic equations of the constitutively non-linear behaviour. For soft biological tissues it is common to adapt the framework of hyperlasticity, based on the definition of a strain energy density function Ψ. To account for quasi-incompressiblity, we additively decompose this strain energy density function into volumetric and isochoric parts, [24]

$$\Psi = \Psi_{vol}(J) + \Psi_{iso}(\bar{\mathbf{C}}). \tag{6}$$

From the evaluation of the dissipation inequality [1, 21], we obtain the second Piola-Kirchhoff stress [24],

$$\mathbf{S} = 2\partial_{\mathbf{C}}\Psi_{vol} + 2\partial_C \Psi_{iso}(\mathbf{C}) = \mathbf{S}_{vol} + \mathbf{S}_{iso} \tag{7}$$

which consists of a volumetric part [24]

$$\mathbf{S}_{vol} = 2\partial_{\mathbf{C}}\Psi_{vol} = J\partial_J \Psi_{vol}\mathbf{C}^{-1} \tag{8}$$

and an isotropic part [24]

$$\mathbf{S}_{iso} = 2\partial_{\mathbf{C}}\Psi_{iso} = 2\partial_{\bar{\mathbf{C}}}\Psi_{iso} : \partial_{\mathbf{C}}\bar{\mathbf{C}} = J^{-2/3}\mathbb{P} : \bar{\mathbf{S}} \tag{9}$$

Here $\bar{\mathbf{S}} = 2\partial_{\bar{\mathbf{C}}}\Psi_{iso}$ is the fictitious second Piola-Kirchhoff stress and $\mathbb{P} = \mathbb{I} - \frac{1}{3}\mathbf{C}^{-1} \otimes \mathbf{C}$ denotes the fourth order projection tensor. Through the contravariant push forward operation, we obtain the Cauchy stress σ, [24]

$$\sigma = \frac{1}{J}\mathbf{F} \cdot \mathbf{S} \cdot \mathbf{F}^t \tag{10}$$

which is typically required for the finite element implementation. The tensor of tangent moduli, a fourth order tensor that relates incremental stresses and strains, is essential for a consistent finite element implementation. It represents the total derivative of the stress $\mathbf{S}$ with respect to the deformation tensor $\mathbf{C}$, [24]

$$\mathbf{C} = 2d_{\mathbf{C}}\mathbf{S} = \mathbf{C}_{vol} + \mathbf{C}_{iso} \tag{11}$$

and consists of a volumetric contribution, [24]

$$\mathbf{C}_{vol} = 2d_{\mathbf{C}}\mathbf{S}_{vol} = 2J\tilde{p}\mathbf{C}^{-1} \otimes \mathbf{C}^{-1} - 2Jp\mathbb{I}_{C^{-1}} \tag{12}$$

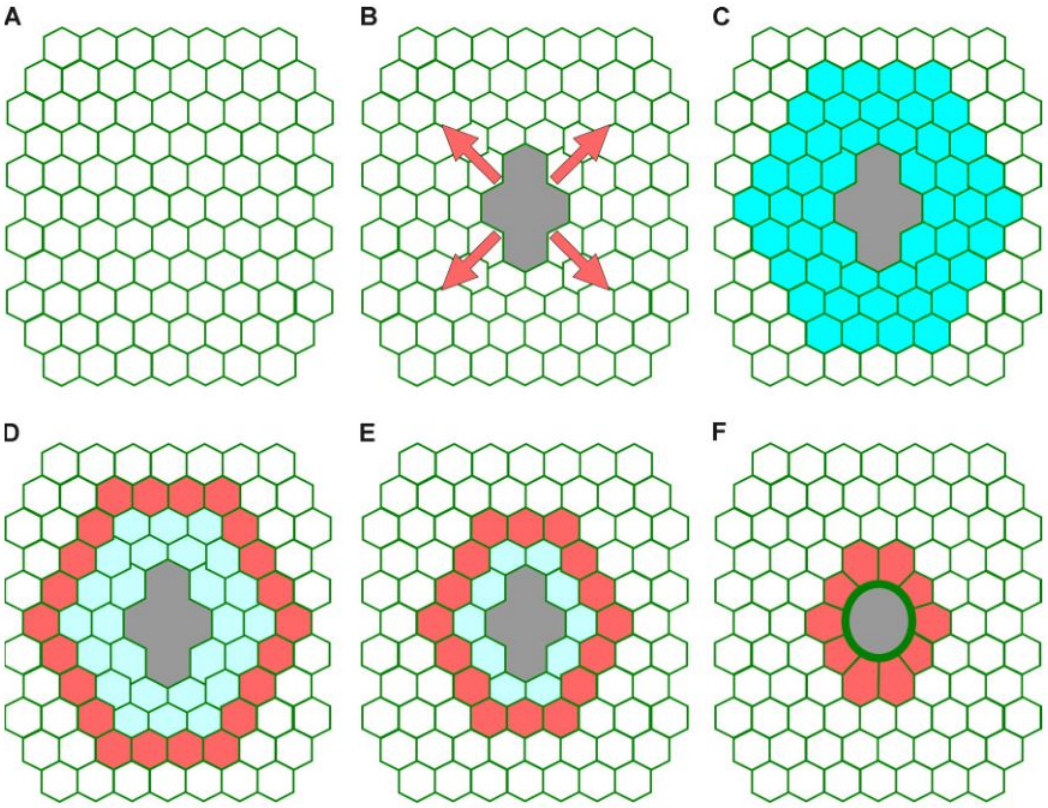

Figure 1: **Graphic model**. Schematic representation of the sequence of events that we propose to occur immediately after wounding simple epithelia.(A) Intact tissue. (B) Wounding released tension and the tissue is displaced from the wound center toward the periphery (arrows). (C) The mechanical stress leads to a burst of intracellular calcium (blue) in the cells that surround the wound. (D) The increase of intracellular calcium (blue) combined with the effects of cell and cytoskeleton deformation determine a region around the wound where a pulse of actin filaments (red) is formed. (E) The actin filaments combined with myosin motors generate an actomyosin flow (red) that travels from cell to cell from the periphery toward the wound margin. (F) When the actomyosin flow reaches the wound margin it contributes to the formation of the wound edge actomyosin cable (green). [3]

and an isochoric contribution [24]

$$\mathbf{C}_{iso} = 2d_{\mathbf{C}}\mathbf{S}_{iso} = \mathbb{P} : \bar{\mathbf{C}} : \mathbb{P}^t + \frac{2}{3}J^{-2/3}tr(\mathbf{S}_{iso})\tilde{\mathbb{P}} \quad (13)$$

$$-\frac{2}{3}[\mathbf{C}^{-1} \otimes \bar{\mathbf{S}} + \bar{\mathbf{S}} \otimes \mathbf{C}^{-1}] \quad (14)$$

Here p denotes the hydrostatic pressure with $\tilde{p} = p + J\partial_J p$, and$\bar{\mathbf{C}} = 4J^{-4/3}\partial_{\bar{\mathbf{C}}\otimes\bar{\mathbf{C}}}\Psi_{iso}$ are the fictitious elastic tangent moduli [12]. In addition, we have introduced the following abbreviations for the fourth order tensors $\tilde{\mathbb{P}} = \mathbb{I}_{\mathbf{C}^{-1}} - \frac{1}{3}\bar{\mathbf{C}} \otimes \bar{\mathbf{C}}$ and $\mathbb{I}_{\mathbf{C}^{-1}} = \frac{1}{2}[\mathbf{C}\bar{\otimes}\mathbf{C} + \mathbf{C}\underline{\otimes}\mathbf{C}]$, where the non-standard fourth order tensor products take the following interpretation, $\{\bullet\}\bar{\otimes}\{\circ\}_{ijkl} = \{\bullet\}_{ik}\{\circ\}_{jl}$ and $\{\bullet\}\underline{\otimes}\{\circ\}_{ijkl} = \{\bullet\}_{il}\{\circ\}_{jk}$.. [24]

2.3 Kinematics of growth

Within the framework of finite growth, the key kinematic assumption is the multiplicative decomposition of the deformation gradient $\mathbf{F}$ into an elastic part $\mathbf{F_e}$ and a growth part $\mathbf{F_g}$ [26].

$$\mathbf{F} = \mathbf{F_e} \cdot \mathbf{F_g} \quad (15)$$

While we can think of the growth tensor $\mathbf{F_g}$ as a second-order variable to characterize arbitrary forms of isotropic or anisotropic growth, here we will parameterize the growth tensor exclusively in terms of a single scalar-valued variable, the growth multiplier θ [13]. This approach is conceptually generic and can be easily adapted to model volume growth, area growth [5], and fiber growth [33]. We denote the Jacobians of the elastic tensor and of the growth tensor as $J_e = det(\mathbf{F_e})$ and $J_g = det(\mathbf{F_g})$, such that [28]

$$J = J_e J_g \quad (16)$$

We can then introduce the elastic right Cauchy Green tensor, [28]

$$\mathbf{C_e} = \mathbf{F_e}^t \cdot \mathbf{F_e} = \mathbf{F_g}^{-t} \cdot \mathbf{C} \cdot \mathbf{F_g}^{-1} \tag{17}$$

and relate it to the total right Cauchy Green tensor $\mathbf{C}$ using the inverse growth tensor.

We specify the growth tensor as

$$\mathbf{F_g} = \mathbf{I} + [1-\theta]\mathbf{n} \otimes \mathbf{n} \tag{18}$$

where θ is the scalar-valued growth multiplier that characterizes the amount of growth and $\mathbf{n}$ is the second principal direction of the deformation gradient. The sensitivity of growth with respect to the growth multiplier then takes the following simple form,

$$\partial_\theta \mathbf{F_g} = \mathbf{n} \otimes \mathbf{n} \tag{19}$$

2.4 Growth driven by volume change

2.4.1 Constitutive equations

We embed the kinematic characterization of growth into the hyperelastic baseline description introduced in Section 2.2. To this end, we reparameterize the free energy function $\Psi(\mathbf{C_e})$, which was initially parameterized in terms of the elastic deformation tensor $\mathbf{C_e}$, in terms of the total deformation tensor $\mathbf{C}$ and the growth tensor $\mathbf{F_g}$, such that $\Psi(\mathbf{C}, \mathbf{F_g})$ and [24]

$$\dot{\Psi} = \partial_{\mathbf{C}} \Psi : \dot{\mathbf{C}} + \partial_{\mathbf{F_g}} \Psi : \dot{\mathbf{F_g}} \tag{20}$$

Thermodynamic considerations motivate the introduction of the second Piola-Kirchhoff stress, [24]

$$\mathbf{S} = 2\partial_{\mathbf{C}} \Psi = 2\partial_{\mathbf{C_e}} \Psi : \partial_{\mathbf{C}} \mathbf{C_e} = \mathbf{F_g}^{-1} \cdot \mathbf{S_e} \cdot \mathbf{F_g}^{-t} \tag{21}$$

Here, $\mathbf{S_e} = 2\partial_{\mathbf{C_e}} \Psi$ is the classic elastic second Piola-Kirchhoff stress as introduced in equation (7). To derive the Lagrangian tangent moduli, essential for a consistent finite element implementation, we evaluate the total derivative of the second Piola-Kirchhoff stress $\mathbf{S}$ with respect to the right Cauchy Green deformation tensor $\mathbf{C}$, [24]

$$\begin{aligned} \mathbf{C} = 2\mathrm{d}_{\mathbf{C}}\mathbf{S} &= \mathbf{C}_\mathrm{e} + \mathbf{C}_\mathrm{g} \\ &= 2\partial_{\mathbf{C}}\mathbf{S}\big|_{\mathbf{F}_\mathrm{g}} + 2\partial_{\mathbf{C}}\mathbf{S}\big|_{\mathbf{F}} \\ &= 2\partial_{\mathbf{C}}\mathbf{S}\big|_{\mathbf{F}_\mathrm{g}} + 2\left[\partial_{\mathbf{F}_\mathrm{g}}\mathbf{S} : \partial_\vartheta \mathbf{F}_\mathrm{g}\right] \otimes \partial_{\mathbf{C}}\vartheta\big|_{\mathbf{F}} \end{aligned} \tag{22}$$

The first term of equation (22) represents the pull back of the elastic tangent moduli to the undeformed reference configuration, [24]

$$\mathbf{C}_\mathrm{e} = 2\mathrm{d}_{\mathbf{C}}\mathbf{S}\big|_{\mathbf{F}_\mathrm{g}} = [\mathbf{F}_\mathrm{g}^{-1}\overline{\otimes}\mathbf{F}_\mathrm{g}^{-1}] : 2\mathrm{d}_{\mathbf{C}_\mathrm{e}}\mathbf{S}_\mathrm{e} : [\mathbf{F}_\mathrm{g}^{-\mathrm{t}}\overline{\otimes}\mathbf{F}_\mathrm{g}^{-\mathrm{t}}]\,. \tag{23}$$

Here, $2d_{\mathbf{C_e}}\mathbf{S_e}$ are the classic elastic tangent moduli as introduced in equation (11). The second term of equation (22) is related to the linearization of the growth model, [24]

$$\mathbf{C}_\mathrm{g} = 2\mathrm{d}_{\mathbf{C}}\mathbf{S}\big|_{\mathbf{F}} = 2\left[\partial_{\mathbf{F}_\mathrm{g}}\mathbf{S} : \partial_\vartheta \mathbf{F}_\mathrm{g}\right] \otimes \partial_{\mathbf{C}}\vartheta\big|_{\mathbf{F}} \tag{24}$$

The first term, $\partial_{\mathbf{F_g}}\mathbf{S}$, is conceptually generic, [24]

$$\begin{aligned} \partial_{\mathbf{F}_\mathrm{g}}\mathbf{S} = &-[\,\mathbf{F}_\mathrm{g}^{-1}\overline{\otimes}\mathbf{S} + \mathbf{S}\underline{\otimes}\mathbf{F}_\mathrm{g}^{-1}\,] \\ &-[\,\mathbf{F}_\mathrm{g}^{-1}\overline{\otimes}\mathbf{F}_\mathrm{g}^{-1}\,] : \tfrac{1}{2}\,\mathbf{C} : [\,\mathbf{F}_\mathrm{g}^{-\mathrm{t}}\overline{\otimes}\mathbf{C}_\mathrm{e} + \mathbf{C}_\mathrm{e}\underline{\otimes}\mathbf{F}_\mathrm{g}^{-\mathrm{t}}], \end{aligned} \tag{25}$$

We define the evolution of the strain driven growth multiplier [24]

$$\dot{\theta} = k(\theta)\phi(\mathbf{C_e}) \tag{26}$$

Where k is a limiting funcion that ensures that the tissue does not grow unboundely [18]

$$k = \frac{1}{\tau}\left[\frac{\theta^{max} - \theta}{\theta^{max} - 1}\right]^\gamma \tag{27}$$

with $\partial_\theta k = -\gamma k/[\theta^{max} - \theta]$. Growth evolves in time according to three parameters, the maximum amount of growth θ^{max}, the adaptation speed τ, and the nonlinearity of the growth process γ.
The growth criterion [5]

$$\phi(\mathbf{C_e}) = \lambda_e - \lambda_{crit} \tag{28}$$

with $\lambda_e = [\mathbf{n}\cdot\mathbf{C_e}\cdot\mathbf{n}]^{1/2}$. Here λ_{crit} denotes a physiological stretch above which growth occurs and $\mathbf{n}$ is a principal direction.

2.4.2 Numerical implementation

For the numerical implementation, we integrate the evolution of growth in time using an implicit Euler backward scheme

$$\dot{\theta} = [\theta^{n+1} - \theta^n]/\Delta t \tag{29}$$

where Δt denotes the current time increment. This allows us to introduce the discrete local residual,

$$\mathcal{R} = \theta^{n+1} - \theta^n - k(\theta)\phi(\mathbf{C_e})\Delta t \tag{30}$$

To solve this non-linear equation, we expand the residual up to the first order term. We can then solve this equation, $\mathcal{R} + \partial_\theta \mathcal{R}\Delta\theta = 0$, within an iterative Newton-Raphson scheme. With the tangent of the residual,

$$\mathcal{K} = \partial_\theta \mathcal{R} = 1 - [k\partial_\theta\phi + \partial_\theta k\phi]\Delta t$$

we can incrementally update the growth multiplier $\theta^{n+1} \leftarrow \theta^n - \mathcal{R}/\mathcal{K}$ until the residual $\mathcal{R}$ has converged towards a small enough user-defined tolerance. Table 1 summarizes the local algorithmic treatment of the numerical procedure, which can be easily embedded into any finite element setting at the constitutive level.

Input: $\mathbf{F}^{t+1}, \theta^t$

1. Compute different kinematic variables: $\mathbf{C}^{t+1}, \mathbf{F}_e^{t+1} = \mathbf{F}^{t+1} \cdot \mathbf{F}_g^t$ and consitutive variables $\mathbf{S}^{t+1}, \mathbf{S}_e^{t+1}$
2. Check for growth
   IF $(\lambda > \lambda_{\text{crit}})$ THEN Determine new growth multiplier
   WHILE $\mathcal{R} > Tol$
   Calculate residual
   $$\mathcal{R} = \theta^{\text{n}+1} - \theta^{\text{n}} - \kappa(\theta)\phi(\boldsymbol{\Xi})\Delta t, \tag{31}$$
   Calculate tangent
   $$\mathcal{K} = 1 - \left[\kappa\partial_\theta\phi + \theta\partial_\theta\kappa\right]\Delta t \tag{32}$$
   Update growth
   $$\theta^{\text{n}+1} \leftarrow \theta^{\text{n}} - \mathcal{R}/\mathcal{K} \tag{33}$$
   END
3. Compute Cauchy stresses σ^{t+1}
   Compute tangent moduli $\mathbf{C}^{t+1}$

Output: $\boldsymbol{\sigma}^{t+1}, \mathbf{C}^{t+1}, \theta^{n+1}$

Table 1: Algorithm for a implicit Euler scheme of volumetric growth

2.5 Growth driven by density change

2.5.1 Constitutive equations

In this case the growth is dependent on the density of actin ρ_{act} in the tissue well as the material density ρ . We define the total strain energy as

$$\Psi = \rho\Psi^{neo} + \rho_{act}\Psi^{act} \tag{34}$$

involving Ψ^{neo}, a classical Neo-Hookean strain energy, and adding a second one Ψ^{act} to account for the reaction of the tissue to the presence of actin. The neo-hookean part of the energy is defined by the equation

$$\Psi_0^{neo} = \frac{\lambda}{2}ln(J)^2 + \frac{G}{2}(I_1 - n_{dim} - 2ln(J)) \tag{35}$$

where λ and G are the first Lamme parameter and shear modulus of the material respectively, J is the jacobian for the total strain, the first invariant of the Cauchy-Green deformation tensor is $I_1 = tr(\mathbf{C})$ and n_{dim} is the number of dimensions considered. The other part of the energy follows the following equation

$$\Psi_0^{act} = \tag{36}$$

The variation of the tissue density is defined by the following expression

$$\dot{\rho} = \left[\frac{\rho}{\rho_0}\right]^{n-m}\Psi - \Psi_0 \tag{37}$$

Where ρ_0 is the initial density, n, m and Ψ_0 are material properties. The variation of the actin density is defined by the mass source R_0, which is a function of the first strain invariant

$$\dot{\rho}_{act} = R_0(\mathbf{C}) = f(I_1) \tag{38}$$

2.5.2 Numerical implementation

For the numerical implementation, we integrate the evolution of density parameter in time using an implicit Euler backward scheme

$$\dot{\rho} = [\rho^{n+1} - \rho^n]/\Delta t \tag{39}$$

$$\dot{\rho}_{act} = [\rho_{act}^{n+1} - \rho_{act}^n]/\Delta t \tag{40}$$

The evolution of the tissue density is calculated using a residual form

$$\mathcal{R} = \rho^{n+1} - \rho^n - \left(\left[\frac{\rho^{n+1}}{\rho_0}\right]^{n-m}\Psi_0^{neo} - \Psi_0\right)\Delta t \tag{41}$$

and its increment

$$\mathcal{K} = 1 - (n-m)\left[\frac{\rho^{n+1}}{\rho_0}\right]^{n-m}\frac{\Psi_0^{neo}}{\rho^{n+1}}\Delta t \tag{42}$$

we can incrementally update the density parameter $\rho^{n+1} \leftarrow \rho^n - \mathcal{R}/\mathcal{K}$ until the residual $\mathcal{R}$ has converged towards a small enough user-defined tolerance. Table 2 summarizes the local algorithmic treatment of the numerical procedure, which can be easily embedded into any finite element setting at the constitutive level.

Input: $\mathbf{F}^{t+1}, \rho^t$

1. Compute different kinematic variables: $\mathbf{C}^{t+1}$ and Ψ_0^{neo}
2. Check for growth
   IF ($\Psi_0^{neo} > tol$) THEN Determine new density parameter
   WHILE $\mathcal{R} > Tol$
   Calculate residual
$$\mathcal{R} = \rho^{n+1} - \rho^n - \left(\left[\frac{\rho^{n+1}}{\rho_0} \right]^{n-m} \Psi_0^{neo} - \Psi_0 \right) \Delta t, \tag{43}$$
   Calculate tangent
$$\mathcal{K} = 1 - (n-m) \left[\frac{\rho^{n+1}}{\rho_0} \right]^{n-m} \frac{\Psi_0^{neo}}{\rho^{n+1}} \Delta t \tag{44}$$
   Update growth
$$\rho^{n+1} \leftarrow \rho^n - \mathcal{R}/\mathcal{K} \tag{45}$$
   END
3. Compute Cauchy stresses σ^{t+1}
   Compute tangent moduli $\mathbf{C}^{t+1}$

Output: $\boldsymbol{\sigma}^{t+1}, \mathbf{C}^{t+1}, \rho^{n+1}$

Table 2: Algorithm for a implicit Euler scheme of volumetric growth

2.6 Results

In order to test the growth model, a 2D symmetric mesh was created. To avoid ill-conditioned elements due to the large deformations, elongated quadrilaterals were introduced near the gap that simulates the wound, as it can be observed in Figure 2.

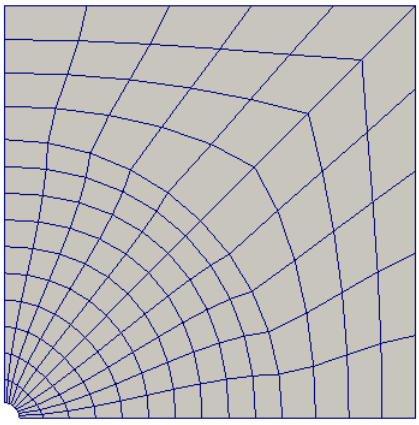

Figure 2: **Finite Element Mesh**

.

Initially, a free deformation with no evolution of the internal variable is performed, to simulate the initial wound opening due to the appearance of an initial gap. In Figure 3 it can be observed the opening of the wound and the concentration of the deformation gradient near the border of the hole when prescribed uniform displacements are applied in the opposite borders.

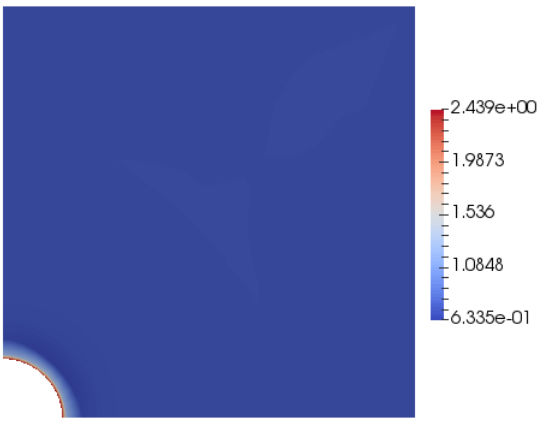

Figure 3: **Initial deformation stage, deformation gradient**

.

Once the initial expansion is done, with no additional external loads applied, shrinking due to volume or den-

sity change can be observed.

2.7 Discussion

Up to the moment this report was written, the separate implementation of the non-elastic mechanics with volume/density growth and a diffusion model for the actin flow were developed. The behaviour of the models is yet to be tested by using the results of the diffusion problem as inputs for the internal variable evolution.

That been said, the model behaves as expected, although tunning of the material constants is yet to be done. The expansion of the hole is done with no need of growth, and the mesh deformation is only function of the initial geometry.

The volume changing growth parameter shows a correlation with the deformation gradient, obtaining reductions in the internal variable when the gradient is larger. The density changing model behaves also well with increase of the actin density when the gradient is bigger.

It is important to remark that this particular model is relevant only for the initial stages of the wound repair process, when the flow of substances seems to be decoupled with the closure of the wound. A fully coupled model is yet to be done to simulate the posterior stages of the phenomena.

References

[1] Gerhard A. Holzapfel . *Nonlinear Solid Mechanics: A Continuum Approach for Engineering*. John Wiley & Sons, 2000.

[2] E. Anon, X. Serra-Picamal, P. Hersen, N. C. Gauthier, M. P. Sheetz, X. Trepat, and B. Ladoux. Cell crawling mediates collective cell migration to close undamaged epithelial gaps. *Proceedings of the National Academy of Sciences*, 109(27):10891–10896, July 2012.

[3] Marco Antunes, Telmo Pereira, Joo V. Cordeiro, Luis Almeida, and Antonio Jacinto. Coordinated waves of actomyosin flow and apical cell constriction immediately after wounding. *The Journal of Cell Biology*, 202(2):365–379, July 2013.

[4] William M. Bement, Craig A. Mandato, and Mary N. Kirsch. Wound-induced assembly and closure of an actomyosin purse string in Xenopus oocytes. *Current Biology*, 9(11):579–587, June 1999.

[5] Adrin Buganza Tepole, Christopher Joseph Ploch, Jonathan Wong, Arun K. Gosain, and Ellen Kuhl. Growing skin: A computational model for skin expansion in reconstructive surgery. *Journal of the Mechanics and Physics of Solids*, 59(10):2177–2190, October 2011.

[6] Joo V. Cordeiro and Antnio Jacinto. The role of transcription-independent damage signals in the initiation of epithelial wound healing. *Nature Reviews Molecular Cell Biology*, 14(4):249–262, February 2013.

[7] L. M. Crosby and C. M. Waters. Epithelial repair mechanisms in the lung. *AJP: Lung Cellular and Molecular Physiology*, 298(6):L715–L731, June 2010.

[8] O. du Roure, A. Saez, A. Buguin, R. H. Austin, P. Chavrier, P. Silberzan, and B. Ladoux. Force mapping in epithelial cell migration. *Proceedings of the National Academy of Sciences*, 102(7):2390–2395, February 2005.

[9] Gabriel Fenteany, Paul A Janmey, and Thomas P Stossel. Signaling pathways and cell mechanics involved in wound closure by epithelial cell sheets. *Current Biology*, 10(14):831–838, July 2000.

[10] P. J. Flory. Thermodynamic relations for high elastic materials. *Transactions of the Faraday Society*, 57:829, 1961.

[11] T. C. Gasser and G. A. Holzapfel. A rate-independent elastoplastic constitutive model for biological fiber-reinforced composites at finite strains: continuum basis, algorithmic formulation and finite element implementation. *Computational Mechanics*, 29(4-5):340–360, October 2002.

[12] T. C. Gasser, R. W Ogden, and G. A Holzapfel. Hyperelastic modelling of arterial layers with distributed collagen fibre orientations. *Journal of The Royal Society Interface*, 3(6):15–35, February 2006.

[13] Serdar Gktepe, Oscar John Abilez, and Ellen Kuhl. A generic approach towards finite growth with examples of athlete's heart, cardiac dilation, and cardiac wall thickening. *Journal of the Mechanics and Physics of Solids*, 58(10):1661–1680, October 2010.

[14] M. S. Hutson. Forces for Morphogenesis Investigated with Laser Microsurgery and Quantitative Modeling. *Science*, 300(5616):145–149, April 2003.

[15] A. Jacinto J. Cordeiro. The role of transcription-independent damage signals in the initiation of epithelial wound healing. *Nature Reviews Molecular Cell Biology*, 14:249–262, April 2013.

[16] Antonio Jacinto, Alfonso Martinez-Arias, and Paul Martin. Mechanisms of epithelial fusion and repair. *Nature Cell Biology*, 3(5):E117–E123, May 2001.

[17] Antonio Jacinto, Sarah Woolner, and Paul Martin. Dynamic Analysis of Dorsal Closure in Drosophila. *Developmental Cell*, 3(1):9–19, July 2002.

[18] V.A. Lubarda and A. Hoger. On the mechanics of solids with a growing mass. *International Journal of Solids and Structures*, 39(18):4627–4664, September 2002.

[19] Eliana Marinari, Aida Mehonic, Scott Curran, Jonathan Gale, Thomas Duke, and Buzz Baum. Live-cell delamination counterbalances epithelial growth to limit tissue overcrowding. *Nature*, 484(7395):542–545, April 2012.

[20] Paul Martin and Julian Lewis. Actin cables and epidermal movement in embryonic wound healing. *Nature*, 360(6400):179–183, November 1992.

[21] A. Menzel. Modelling of anisotropic growth in biological tissues: A new approach and computational aspects. *Biomechanics and Modeling in Mechanobiology*, 3(3):147–171, March 2005.

[22] T. Omelchenko, J. M. Vasiliev, I. M. Gelfand, H. H. Feder, and E. M. Bonder. Rho-dependent formation of epithelial "leader" cells during wound healing. *Proceedings of the National Academy of Sciences*, 100(19):10788–10793, September 2003.

[23] M. Poujade, E. Grasland-Mongrain, A. Hertzog, J. Jouanneau, P. Chavrier, B. Ladoux, A. Buguin, and P. Silberzan. Collective migration of an epithelial monolayer in response to a model wound. *Proceedings of the National Academy of Sciences*, 104(41):15988–15993, October 2007.

[24] E. Pea P.Saez. Computational modeling of hypertensive growth in the human carotid artery. *Computational Mechanics*, 53(6):1183–1196, 2014.

[25] Andrea Ravasio, Ibrahim Cheddadi, Tianchi Chen, Telmo Pereira, Hui Ting Ong, Cristina Bertocchi, Agusti Brugues, Antonio Jacinto, Alexandre J. Kabla, Yusuke Toyama, Xavier Trepat, Nir Gov, Lus Neves de Almeida, and Benoit Ladoux. Gap geometry dictates epithelial closure efficiency. *Nature Communications*, 6:7683, July 2015.

[26] E. K. Rodriguez, A. Hoger, and A. D. McCulloch. Stress-dependent finite growth in soft elastic tissues. *Journal of Biomechanics*, 27(4):455–467, April 1994.

[27] Jody Rosenblatt, Martin C. Raff, and Louise P. Cramer. An epithelial cell destined for apoptosis signals its neighbors to extrude it by an actin- and myosin-dependent mechanism. *Current Biology*, 11(23):1847–1857, November 2001.

[28] Pablo Sez, Estefania Pea, Miguel Angel Martnez, and Ellen Kuhl. Computational modeling of hypertensive growth in the human carotid artery. *Computational Mechanics*, 53(6):1183–1196, June 2014.

[29] T. J. Shaw and P. Martin. Wound repair at a glance. *Journal of Cell Science*, 122(18):3209–3213, September 2009.

[30] Kevin J. Sonnemann and William M. Bement. Wound Repair: Toward Understanding and Integration of Single-Cell and Multicellular Wound Responses. *Annual Review of Cell and Developmental Biology*, 27(1):237–263, November 2011.

[31] Masako Tamada, Tomas D. Perez, W. James Nelson, and Michael P. Sheetz. Two distinct modes of myosin assembly and dynamics during epithelial wound closure. *The Journal of Cell Biology*, 176(1):27–33, January 2007.

[32] Xavier Trepat, Michael R. Wasserman, Thomas E. Angelini, Emil Millet, David A. Weitz, James P. Butler, and Jeffrey J. Fredberg. Physical forces during collective cell migration. *Nature Physics*, 5(6):426–430, June 2009.

[33] Alexander M. Zllner, Oscar J. Abilez, Markus Bl, and Ellen Kuhl. Stretching Skeletal Muscle: Chronic Muscle Lengthening through Sarcomerogenesis. *PLoS ONE*, 7(10):e45661, October 2012.